



HAL
open science

Stochastic simulation of urban environments

Thomas Courtat, Laurent Decreusefond, Philippe Martins

► **To cite this version:**

Thomas Courtat, Laurent Decreusefond, Philippe Martins. Stochastic simulation of urban environments: Application to Path-loss in wireless systems. 2014. hal-01297890

HAL Id: hal-01297890

<https://hal.science/hal-01297890>

Preprint submitted on 5 Apr 2016

HAL is a multi-disciplinary open access archive for the deposit and dissemination of scientific research documents, whether they are published or not. The documents may come from teaching and research institutions in France or abroad, or from public or private research centers.

L'archive ouverte pluridisciplinaire **HAL**, est destinée au dépôt et à la diffusion de documents scientifiques de niveau recherche, publiés ou non, émanant des établissements d'enseignement et de recherche français ou étrangers, des laboratoires publics ou privés.



Distributed under a Creative Commons Attribution - NonCommercial - ShareAlike 4.0 International License

Stochastic simulation of urban environments Application to Path-loss in wireless systems

Thomas Courtat^a, Laurent Decreusefond^a, Phillipe Martins^a

^a*Télécom ParisTech, 23 avenue d'Italie, 75013 Paris, France*

Abstract

We are interested in the assessment of electromagnetic Path-Loss in complex environments. The Path-loss is the attenuation function P of the electromagnetic power at a distance d of an antenna. In free-space, $P(d) \propto 1/d^2$, in complex environments like cities, wave trajectory is altered by successive reflections and absorptions, the path-loss is not theoretically known and engineering rules postulate that $P(d) \simeq 1/d^\gamma$, $\gamma > 2$.

We place in a stochastic geometry context to answer the problem statistically. We present random models of 3D-city. These models reproduce main real cities' features, can be calibrated with simple mean formulae and can be fast simulated. For collections of random cities with the same mean morphology, we estimate by Monte-Carlo ray tracing techniques their attenuation maps. By averaging these maps, we show that the power expectancy actually follows a function $\sim 1/d^\gamma$ with γ depending on the environment morphology.

Keywords: Stochastic Geometry, Monte-Carlo, Simulation, Path-loss, Telecommunication

1. Introduction

In this paper, we seek out to analyze quantitatively the power field generate by an electromagnetic source over a complex urban environment.

In the ideal case of free space propagation, the power $\mathbf{P}(d)$ at a point only depends on its distance d to the source: $\mathbf{P}(d) \propto 1/d^2$. In a urban environment, the power field in a point is constituted by a multitude of paths created by successive reflections of source waves on the buildings of the city. Qualitative and empirical engineering rules are applied to assess the power's order of magnitude [17]. The formula that is commonly admitted is $\mathbf{P}(d) = \frac{c}{d^\alpha} \cdot H$ with $2 < \alpha \leq 4$ depending on the specificity of the environment under consideration and H a random variable following a Rayleigh or log-normale law, independent to the distance, to account the interference fading and the shadowing (zones that are partially or totally darkened by elements of the landscape).

The synthetic knowledge of this exponent is of main interest in planning and sizing of wireless telecommunication networks.

We present here a statistical approach to solve this problem. Rather than trying to determine the precise attenuation map for a particular city, we build representative stochastic models for cities and explore the statistical properties of the random attenuation map in each model.

From a deterministic point of view, the regular square lattice, the "Manhattan" model is often used [19] to represent the street network. But this model very particular geometrical features that do not give a full account of the variability of morphologies that are observed between real cities.

Stochastic geometry [18, 20], allows proposing random models of planar network [3, 1, 11] and to calculate statistical indicators to answer various planning problems. We can for instance cite the coverage probability of a cellular network with or without user displacement [13] or the length distribution in a cooper or optical network [10].

The outline of stochastic approach is to describe in one hand the city (yet restricted to its street network in the literature) by a small number of parameters (as the street density, the mean number of intersections

by $\text{km}^2\dots$) and in the other hand the structure of the telecommunication network by another small set of parameters (the spatial density of routers, of users...). Theoretical models of networks (Poisson Line, Poisson Voronoï, or Poisson Delaunay [7]) and spatial point distribution models (Poisson Processes, Cox Processes [3, 8, 13]) allow simulating collections of cases with the same statistical properties ; the statistical answer to the problem under consideration is then obtained by evaluating the expectancy of relevant functional over these collections. In some problems or limit cases, this evaluation can be made from analytical calculation [21] or be rewritten as real valued function integrals one just has to compute numerically [13].

As for Path-loss function problem, a ray tracing approach [4] has been presented in [12]. The retained city model is a square lattice with percolation: each site is occupied by a building with a given probability. The electromagnetic wave propagates from a punctual source in the horizontal plane by reflecting on buildings. One of their key point to estimate power field is that as it reflects a ray performs a recurrent random walk. Yet if a random walk is recurrent in the plane, this phenomenon does not happen in dimension three. We thus can expect different results if we take the three dimensional structure of the city into account.

The first step of this article presents three dimensional random models for cities, both tractable and realistic. They mimic main features of cities: facades alignment along streets, organization of buildings into blocks, variability in the topology of street intersections and of the network anisotropy [5]. We proceed into two parts: at first we generate street axis from random tessellations (Sec.2), secondly we add random buildings in the cells of the tessellation (Sec.3).

The second step is the probabilistic modelling of propagation and the realization of an efficient Monte-Carlo ray tracing algorithm to evaluate the power field generated by an antenna placed in height (Sec.4).

From this point, we can simulated classes of statistically equivalent cities and compute the power field also called attenuation map and estimate the expectancy of the received power at a distance d of an antenna (Sec.5).

The algorithms are efficiently implemented under our *GeoStat* framework. Every step of the simulations is done with vector objects: to avoid aliasing effects, buildings are collections of polytopes and the maps are never rasterized. Algorithms we present are optimized, the main point of algorithms are present through the article body and their technical refinement are sent back to annexes (Appendix B.3). Their need in memory and running time are discussed in (Appendix B.4).

2. Street Models

2.1. General definitions

Definition 1 (Directed line). In the Euclidian plane, a directed line L is defined by its origin o_L and its direction vector u_L .

The set of lines in the plane is written \mathbb{H}

Definition 2 (Line). If L is a directed line then $|L| = \{o_L + \lambda u_L, \lambda \in \mathbb{R}\}$ is a subset of \mathbb{R}^2 called a line. The set of lines is written $|\mathbb{H}|$.

A line L is unequivocally defined by $\pi_L(o)$ the projection of the origin 0 of the plane over L i.e by a signed distance to the origin and a geometric angle with the x -axis. Thus $|\mathbb{H}|$ is seen as the cylinder $\mathbb{R} \times [0, \pi[$.

A directed line L divides \mathbb{R}^2 into two disconnected parts: $L_+ = \{x \in \mathbb{R}^2, \det(u_L, (x - o_L)) > 0\}$ and $L_- = \{x \in \mathbb{R}^2, \det(u_L, (x - o_L)) < 0\}$.

From this remark, we adopt the following general recursive definition of polygons:

Definition 3 (Polygons). The set of polygons \mathbb{P} is the subset of convex bodies \mathbb{K} defined by $\mathbb{P} = \bigcup_n \mathbb{P}_n$ with $\mathbb{P}_0 = \{\mathbb{R}^2\}$ and $\forall n > 0, \mathbb{P}_n = \{P \in \mathbb{K}, \exists Q \in \mathbb{P}_{n-1} \text{ and } L \in \mathbb{H}, P = Q \cap L_+ \text{ or } P = Q \cap L_-\}$

Definition 4 (Tessellation and cells). A (straight convex) tessellation Ξ is a countable family of convex polygons $\{C_i\}_{i \in \mathbb{N}}$ (the cells) partitioning \mathbb{R}^2 and whose interiors do not intersect.

For instance, if $X = \{X_i\}$ is a countable family of points in the plane, to each point X_i is associated is Voronoï zone $V(X_i|X)$. Then $\{V(X_i|X)\}_i$ is a tessellation.

To the border $\partial \Xi = \cup \partial C_i$ of a tessellation is associated a straight planar graph denoted $\mathcal{G}(\partial \Xi)$ whose vertices are the cells' vertices and edges are cell's.

Definition 5 (Axis). Two edges of $\mathcal{G}(\partial\Xi)$ are aligned if they are equal or intersect and make a 0 angle. The alignment relationship is symmetric.

The transitive closure of the alignment relationship generates a partition of $\partial\Xi$ deprived of the $\mathcal{G}(\partial\Xi)$'s vertices into sets composed of one segment, one line or one half-lines. These sets are called axis.

2.2. Elements of random geometry

Definition 6 (General Poisson Point Process). If Ω is a Polish Space equipped with a Borelian measure Λ , there exists a countable point process $X = \sum X_i \in \Omega$ such that:

1. If K_1 and K_2 are two measurable sets of Ω that do not intersect then $X \cap K_1$ and $X \cap K_2$ are independent point processes.
2. If K is a compact of Ω , the number of points of X in K is a random variable with a Poisson distribution: $\#X \cap K \sim \mathcal{P}(\Lambda(K))$

For instance in \mathbb{R}^n with $\Lambda(\cdot) = \lambda \cdot \mu(\cdot)$, μ being the Lebesgue's measure and λ a positive real number we obtain the "stationary" Poisson Point Process of intensity λ

Definition 7 (Poisson Line (PL)). The Poisson Line Process (PL) $\partial\Xi$ of intensity measure λ and anisotropy probability measure \mathcal{R} is the Poisson Point Process on the cylinder $\mathbb{R} \times [0, \pi[= |\mathbb{H}|$ of intensity $\mathcal{L}(\cdot) = \lambda\mu(\cdot) \otimes \mathcal{R}(\cdot)$, $\lambda > 0$.

Theorem 1 (Random Line). If W is a compact set in the plane then $\mathcal{L}_W(\cdot) = \mathcal{L}(\{h \in \mathcal{H}, h \cap W \neq \emptyset\}) < \infty$. A Uniform Random Line in W is a random variable on $|\mathbb{H}|$ with distribution $\mathbb{U}_W = \frac{\mathcal{L}_W(\cdot)}{\mathcal{L}_W(|\mathbb{H}|)}$

Theorem 2 (Random Tessellation). Equipped with the σ -algebra generated by sets $\{\Xi, \partial\Xi \cap K = \emptyset\}$ where K is any compact subset of \mathbb{R}^2 , the set of tessellation is measurable [11].

Let thus Ξ be a random tessellation. Its intensity function is the measure defined by $L_A(W) \stackrel{\text{def}}{=} \mathbb{E}(\mu_1(\Xi \cap W))$ for any compact W .

A random tessellation may be deduced from a point a random point process. For instance, $X = \sum X_i$ if is a Poisson Point Process in the plane, then $\{V(X_i|X)\}_i$ is a random tessellation named Poisson Voronoï Tessellation [18].

Definition 8. A random tessellation Ξ is stationary if $\Xi + \vec{v} \stackrel{\text{dist}}{=} \Xi$, $\forall \vec{v} \in \mathbb{R}^2$.

Definition 9. A random tessellation is locally finite if $L_A(W) < \infty$, $\forall W$ compact.

2.3. Poisson Line Tessellation and Crack STIT Tessellation

Model choice. Poisson Voronoï Tessellations as other theoretically well known models have been suggested to represent street systems [7, 9].

Two models are particularly relevant to model street systems: Poisson Line Tessellation [18, 13, 11] and Crack STIT Tessellation [14].

It has been shown in [5, 16] that a city's morphology can result from two growth mechanisms. The first one is an organic like growth: independent agents divide sequentially plots of land to settle in. Agents do not consult each other, consequently axis they create are not coherent and street intersections are T-shaped. Conversely in the case of a planned growth, agents act under the authority and draw long transportation axis to optimize displacements within the city. Crack Stit tessellations mimic the organic case and Poisson Line Tessellations the planned one (Fig.1).

Moreover these two models are quite similar and can be treated in the same framework. Indeed they both result from sequential divisions of polygons and if edges in a Crack Stit were extended into infinite line, one would obtain a Poisson Line Tessellation. This has for consequence that the typical cell of the tessellations are equal in distribution ([15]).

They both depend on two parameters: an intensity parameter $\lambda \in \mathbb{R}_+$ and a probability measure over $[0, \pi]$, \mathcal{R} that describes the anisotropy of the street system.

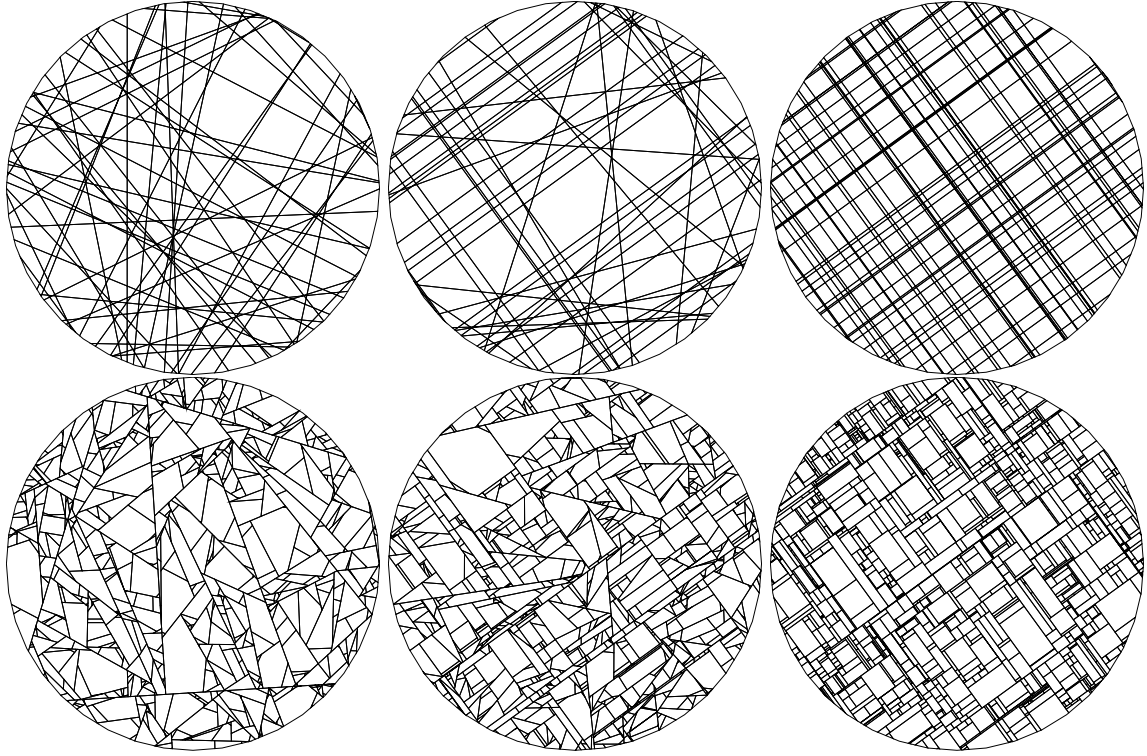


Figure 1: Realization of tessellations into a disc. The first row shows PLT with from left to right an anisotropy of 0, 0.5 and 1. The second row shows Crack STIT with the same anisotropy distributions.

Poisson Line Tessellation.

Definition 10 (Poisson Line Tessellation). If $\partial\Xi$ is a Poisson Line Process then the Poisson Line Tessellation (PLT) Ξ is the set of connected components of $\mathbb{R}^2 \setminus \partial\Xi$.

Crack STIT Tessellation. A Crack is the result of a sequential random division of the plane. Informally, at a time t , the tessellation is $\Xi_t = \{C_i\}$ and dt , each cell C_i in the tessellation has a probability $\lambda \nu(C_i).dt$, $\lambda > 0$ to be divided into two new cells and a probability $o(dt^2)$ to be divided twice. $\nu(\cdot)$ is a positive measure on the set of convex bodies, invariant under rigid motion (for instance area, perimeter, number of vertices) [6]. The tessellation is observed at a finite time τ , the homogeneous quantity $\lambda.\tau$ describes the intensity of the process in the such a way one can come down to $\tau = 1$. If the measure ν is the perimeter (which is the case under consideration in what follows), the resulting tessellation process has interesting properties: it is STable under ITERation (STIT) and its typical cell is equal in distribution to the PLT's one.

Definition 11 (Binary tree). Let $0, +, -$ be three symbols and let's define recursively the sets A_n by: $A_0 = \{(0)\}$ and $\forall n > 0$, $A_n = \{(a, +)\} \cup \{(a, -)\}$, $a \in A_{n-1}$.

The rooted binary tree A is defined by $A = \cup A_n$.

If $a \in A$ then $a_+ = (a, +) \in A$ and $a_- = (a, -) \in A$ are the daughters of a .

Conversely, if $b \in A, b \neq 0, \exists a \in A, b$ is a daughter of a .

Definition 12 (Finite division process). Let W a compact set of the plane A the rooted binary tree and $\lambda, \tau \in \mathbb{R}_+^*$

c is a random polygon process, l a random line process, T and ΔT random real number process ; they are all indexed by the elements of A and are defined recursively:

$$\begin{cases} c(0) = W, T(0) = 0 \\ \Delta T(a) \sim \mathcal{E}(\lambda|c(a)|), \forall a \in A \\ l(a) \sim \mathbb{U}_{C(T(a))}, \forall a \in A \\ c(a_+) = c(a) \cap l(a)_+, \forall a \in A \\ c(a_-) = c(a) \cap l(a)_-, \forall a \in A \\ T(a_+) = T(a_-) = T(a) + \Delta T(a) \forall a \in A \end{cases} \quad (1)$$

from these processes, we define the stochastic polygon process C indexed by $A \times \mathbb{R}_+$

$$C(a, t) = \begin{cases} \emptyset & \text{if } t < T(a) \\ c(a) & \text{if } T(a) \leq t < T(a) + \Delta T(a) \\ \emptyset & \text{if } t \geq T(a) + \Delta T(a) \end{cases} \quad (2)$$

The finite division process of W is the tessellation $\Xi_\tau = \cup_{a \in A} C(a, \tau)$

Definition 13 (Crack STIT Tessellation). There exists a stationary locally finite tessellation in the plane such as $\forall W$ compact subset, $\Xi \cap W \stackrel{\text{dist}}{=} C_\tau(W)$ [14]. It is called the Crack STIT Tessellation.

Theorem 3. Both PLT and Crack STIT Tessellations are locally finite and stationary.

2.4. Mean formulae

Mean formulae (Tab.1, [15]) are known for topological features of PLT and Crack STIT in a disc of area 1 in function of their intensity λ and of the so called anisotropy parameter:

$$\xi \stackrel{\text{def}}{=} \iint |\sin \angle(u, v)| \mathcal{R}(du) \mathcal{R}(dv) \quad (3)$$

(these formulae remain true for all Borelian of area 1 if the tessellation is isotropic i.e. if \mathcal{R} is uniform or if $\xi = 2/\pi$).

Knowing these mean formulae permits to calibrate the models to fit real data which is of prim interest. For instance in sections 4 and 5 we will chose the intensity of the tessellation such as a block of houses has a perimeter of 400 m in average.

Parameters	Notation	Mean value per u.a for PLT	Mean value per u.a for Crack
Total edge length	L_A	λ	$\lambda \cdot \tau$
Number of vertices	N_0	$\frac{1}{2} \xi \lambda^2$	$L_A^2 \xi$
Number of edges	N_1	$\lambda^2 \xi$	$\frac{3}{2} L_A^2 \xi$
Number of cells	N_2	$\frac{1}{2} \lambda^2 \xi$	$\frac{1}{2} L_A^2 \xi$
Length of the typical edge	U_1	$2/(3\lambda\xi)$	$2/(3L_A\xi)$
Perimeter of the typical cell	U_2	$4/(\lambda\xi)$	$4/(L_A\xi)$
Area of the typical cell	A_2	$2/(\lambda^2\xi)$	$2/(L_A^2\xi)$

Table 1: Expectancies of various morphological features of PLT and Crack STIT in function of their intensity λ and their anisotropy parameter ξ . The notion of "typical" object is very useful in stochastic geometry. It basically corresponds to the idea of an object sampled out of a large collection independently of any measure that can be applied to it (see [2, 18, 20]).

In a city modelling context, the family of angular distributions:

$$\mathcal{R}_\rho = \rho \mathcal{U}_{[0, \pi]} + \frac{(1-\rho)}{2} (\delta_\theta + \delta_{\theta+\pi/2}) \quad (4)$$

. allows to go continuously from an isotropic network ($\rho = 0$) to an anisotropic Manhattan-like one ($\rho = 1$). For this family of distributions, ξ writes:

$$\xi(\rho) = \rho^2 \left(\frac{1}{2} - \frac{2}{\pi} \right) + \frac{2}{\pi} \quad (5)$$

3. Building generation

The tessellation is to represent the street axis (alignments of edges), the city skeleton (Fig.2,1). From this, axis are thickened with a Minkowski's sum \oplus_ϵ , $\epsilon > 0$.

Definition 14. If A is a subset of the plane,

$$\oplus_\epsilon A = \{x \in \mathbb{R}^2, d(x, A) \leq \epsilon\} \quad (6)$$

Theorem 4. If $\{A_i\}$ are the axis of a tessellation, the connected components of $\mathbb{R}^2 \setminus \oplus_\epsilon \cup A_i$, $\epsilon > 0$ are polygons B_i that do not intersect.

If $\{C_i\}$ is the set of cells of the tessellation then each B_i is the image of a cell C_k by the operator

$$\ominus_{\epsilon/2}(C) = \{x \in C, d(x, \partial C) > \frac{\epsilon}{2}\} \quad (7)$$

As a consequence, thickening axis into streets is equivalent to generate building blocks from cells (Fig.2,2) by applying $\ominus_{\epsilon/2}$ independently to each cell in \mathcal{T} .

Once blocks obtained, we associate to each block B its image by the dilatation of center its center of mass and ratio η : \tilde{B} (Fig.2,3).

A Poisson Point Process of intensity $1/(b.\eta)$ is drawn on $\partial\tilde{B}$ (Fig.2,4). Then we project these points on the border of B and apply a computational procedure to create polygons from these two sets of points. Simple but laborious to explain symbolically, this procedure is shown in (Fig.2,5) and permits to draw buildings' footprint.

To each building is associated a random height from a distribution $\mathcal{E}(h)$, $h > 0$

From these tessellations streets models and this building generation method, it is possible to simulate a random urban environment by deciding of:

- It's topology (mainly T intersections of X intersections)
- A mean parameter chosen from Tab.1 to fit the intensity of the model,
- The mean street width,
- The mean number of buildings in a block,
- The mean building height.

These random models define parametric classes of urban environments morphologically equivalent. We present in Appendix B key functions to simulate efficiently a large number of representative environments for each class and set of parameters.

In what follows, we illustrate the interest of these models by studying the environment's mean morphology impact over the path loss function of an electromagnetic wave emanating from a placed-high antenna to any user at the ground level, at a distance d of the antenna. The commonly admitted rule of thumb is that $P(d) \simeq d^{-\alpha}$ with α depending on the environment.

In 4 we settle a probabilistic framework suited to compute the wave propagation by Monte-Carlo / ray tracing methods.

In 5 we implement these methods for several representative morphology classes and a large number of independently generated environments and exhibit statistically the impact of the morphology on the path loss exponent α .

Given a real world map, one can fast assesses fit the map to a statistical model and deduce the corresponding expected α .

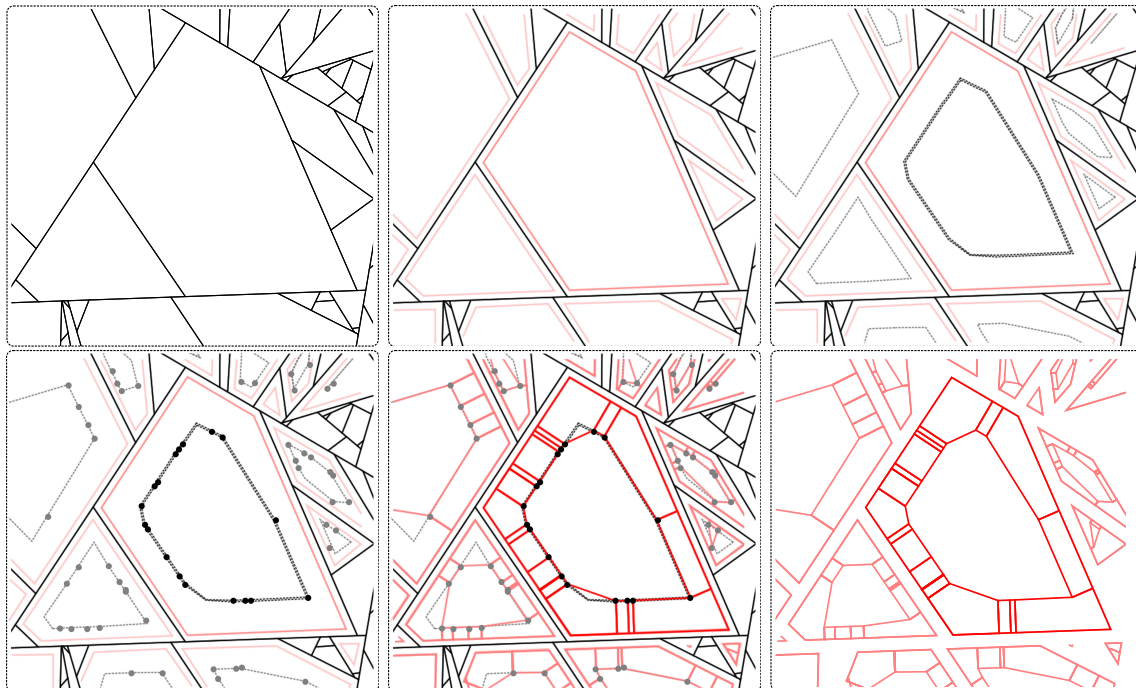


Figure 2: Steps in the building generation. From a tessellation (1) we apply an erosion operator to axis (2) in each new cell, we compute its dilated polygon with respect to its center of mass (3) we draw on this polygon a Poisson Point Process (4) whose points are projected to create buildings' footprint (5)

4. Propagation simulation

4.1. Source antenna model

Given a urban environment, we model a wireless telecommunication antenna by a sphere \mathbb{S} , placed at the center off mass of the nearest roof of the origin of the plane ($\vec{0}$), with an additional height δH .

It is parametrized with spherical coordinates $s = (\theta_{xy}, \theta_z)$ (Fig.3), equipped with its Borel σ -algebra \mathcal{S} and the uniform measure $\mathcal{S}(d\theta_{xy}, d\theta_z) = \frac{1}{4\pi} d\theta_{xy} |\sin(d\theta_z)|$.

It emits in the sphere portion $\Delta\mathcal{S} = [\theta_{xy_0} - \delta\theta_{xy}, \theta_{xy_0} + \delta\theta_{xy}] \times [\theta_{z_0} - \delta\theta_z, \theta_{z_0} + \delta\theta_z]$ of total measure $\mathcal{S}(\Delta\mathcal{S}) = \frac{1}{\pi} \delta\theta_{xy} \sin(\delta\theta_z) \cos(\theta_{z_0})$. The measure restricted to $\Delta\mathcal{S}$ is $\Delta\mathcal{S}(\cdot) \stackrel{\text{def}}{=} \frac{\mathcal{S}(\cdot)}{\mathcal{S}(\Delta\mathcal{S})}$. The power density of the antenna is $P_0 \cdot \Delta\mathcal{S}(\cdot)$ with $P_0 \geq 0$ the total power emanating from the source.

We write ∂E the set of polygons constituting the buildings and the ground of the city. ∂E splits the space \mathbb{R}^3 into three parts: E which is the interior of the buildings and the under-ground where wave cannot propagate, ∂E itself where waves are reflected and $\Omega = \mathbb{R}^3 \setminus (E \cup \partial E)$, an open set whose boundary is ∂E , representing the wave propagation space.

To each $s \in \Delta\mathcal{S}$ is associated $r_s \subset \Omega$ the trajectory of an elementary wave emanating from s . It is assumed that r_s is the result of successive reflections on ∂E respecting the Snell-Descartes rules.

Between its n -th and $n+1$ -th reflection, r_s is a segment denoted $r_s^{(n)}$; $r_s = \cup_n r_s^{(n)}$. If $x \in \Omega \cap r_s^{(n)}$, we write $\vec{r}_s^{(n)}(x)$ the propagation direction of r_s at point x .

When reflected, a portion $1 - \gamma$, $\gamma \in [0, 1]$ of the ray power is absorbed.

We define in the following subsection in probabilistic terms the physical notions of electromagnetic flow, Poynting vector and electromagnetic power.

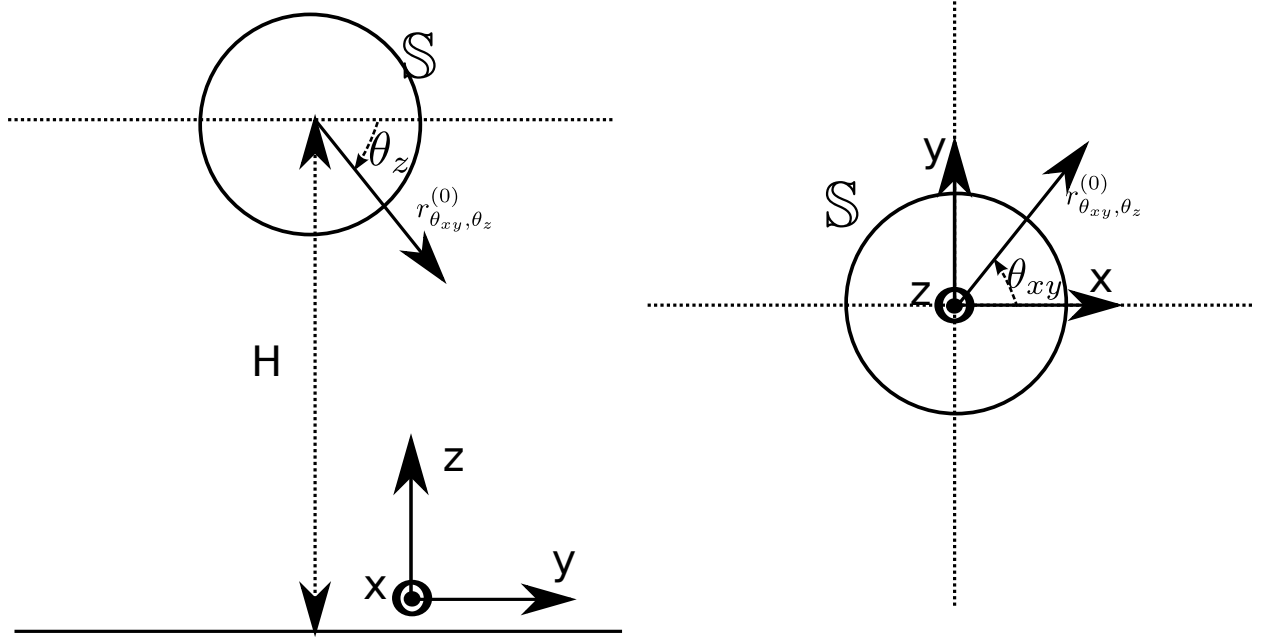


Figure 3: Sketch of the source \mathbb{S} as a sphere observed from the front and from above. One can see the definition of angles θ_z θ_{xy} that identify the first portion of a ray $r_{\theta_{xy}, \theta_z}^{(0)}$.

4.2. Flow, Poyning's vector and power probabilistic definition

We emphasize that \mathbb{S} is compact, separable and connected metric space.

The following assumption is a convenient abstract description of the trajectories of rays from the source \mathbb{S} :

Assumption 1. Let $n \in \mathbb{N}$, $x_0 \in \Omega$ and $s_0 \in \mathbb{S}$.

There exist $\epsilon_{x_0} > 0$ and $\epsilon_{s_0} > 0$ and balls $V_{\epsilon_{x_0}}(x_0) \subset \Omega$, centered in x_0 , of radius ϵ_{x_0} and $V_{\epsilon_{s_0}}(s_0) \subset \mathbb{S}$, centered in s_0 , of radius ϵ_{s_0} such as

- If $x_0 \in r_{s_0}^{(n)}$, $\{r_s^{(n)} \cap V_{\epsilon_{x_0}}(x_0), s \in V_{\epsilon_{s_0}}(s_0)\}$ is homeomorph to $V_{\epsilon_{s_0}}(s_0) \times]0, 1[$
- If $x_0 \notin r_{s_0}^{(n)}$, $\{r_s^{(n)} \cap V_{\epsilon_{x_0}}(x_0), s \in V_{\epsilon_{s_0}}(s_0)\} = \emptyset$

Theorem 5. If $n \in \mathbb{N}$, $x_0 \in \Omega$ then the set $\{s \in \mathbb{S}, x \in r_s^{(n)}\}$ is finite.

In what follows, without more precision, \mathbb{M} is a separable, connected, locally compact manifold in Ω of dimension $\dim \mathbb{M} \leq 2$, C^1 almost everywhere, equipped with its Borel σ -algebra \mathbb{M} and its Borel measure \mathcal{M} .

Definition 15. For all $n \in \mathbb{N}$, $m \in \mathbb{N} \cup \{\infty\}$, $s \in \mathbb{S}$ and $(S, M) \in \mathbb{S} \otimes \mathbb{M}$, we define the sets:

- $q_{\mathbb{M}}^{(n)}(s) = \{x \in \mathbb{M}, x \in r_s^{(n)}\}$
- $R_{\mathbb{M}}^{(n)}(S, M) = \{s \in \mathbb{S}, q_{\mathbb{M}}^{(n)}(s) \neq \emptyset\}$
- $R_{\mathbb{M}}^{(n, m)}(S, M) = \{s \in \mathbb{S}, \#q_{\mathbb{M}}^{(n)}(s) = m\}$

Theorem 6. $\forall n \in \mathbb{N}, \mathcal{S}(R_{\mathbb{M}}^{(n, \infty)}) = 0$

Theorem 7. If $\dim \mathbb{M} \leq 1$, $\forall n \in \mathbb{N}$, $\forall m \in \mathbb{N}$, $\mathcal{S} \left(R_{\mathbb{M}}^{(n,m)} \right) = 0$

Definition 16. We define for $(S, M) \in \mathcal{S} \otimes \mathbb{M}$,

$$\left| \Phi_{\mathbb{M}}^{(n)} \right| (S, M) = \sum_m m \cdot \mathcal{S} \left(R_{\mathbb{M}}^{(n,m)}(S, M) \right) \quad (8)$$

- $\left| \Phi_{\mathbb{M}}^{(n)} \right|$ is a measure over $\mathbb{S} \times \mathbb{M}$
- Moreover, $\left| \Phi_{\mathbb{M}}^{(n)} \right| \ll \mathcal{S} \otimes \mathcal{M}$

In particular, if S is an open set in \mathbb{S} , $\left| \Phi_{\mathbb{M}}^{(n)} \right| (S, \cdot)$ is a measure over \mathbb{M} and $\left| \Phi_{\mathbb{M}}^{(n)} \right| (S, \cdot) \ll \mathcal{M}$

Definition 17. Let's write $\vec{m}(x)$ the orthogonal direction of $\mathbb{M} \ni x$ at point x .

In addition to def. 15, we define for all $n \in \mathbb{N}$, $m \in \mathbb{N} \cup \{\infty\}$, $s \in \mathbb{S}$ and $(S, M) \in \mathcal{S} \otimes \mathbb{M}$, the sets:

- $q_{\mathbb{M},+}^{(n)}(s) = \left\{ x \in r_s^{(n)} \cap \mathbb{M}, \left\langle \vec{r}_s^{(n)}(x) \middle| \vec{m}(x) \right\rangle > 0 \right\}$
- $q_{\mathbb{M},-}^{(n)}(s) = \left\{ x \in r_s^{(n)} \cap \mathbb{M}, \left\langle \vec{r}_s^{(n)}(x) \middle| \vec{m}(x) \right\rangle < 0 \right\}$
- $R_{\mathbb{M},+}^{(n,m)}(S, M) = \left\{ s \in S, \#q_{\mathbb{M},+}^{(n)}(s) = m \right\}$
- $R_{\mathbb{M},-}^{(n,m)}(S, M) = \left\{ s \in S, \#q_{\mathbb{M},-}^{(n)}(s) = m \right\}$

Definition 18. We define for $(S, M) \in \mathcal{S} \otimes \mathbb{M}$,

- $\Phi_{\mathbb{M}+}^{(n)}(S, M) = \sum_m m \cdot \mathcal{S} \left(R_{\mathbb{M}+}^{(n,m)}(S, M) \right)$
- $\Phi_{\mathbb{M}-}^{(n)}(S, M) = \sum_m m \cdot \mathcal{S} \left(R_{\mathbb{M}-}^{(n,m)}(S, M) \right)$

and

$$\Phi_{\mathbb{M}}^{(n)} = \Phi_{\mathbb{M}+}^{(n)} - \Phi_{\mathbb{M}-}^{(n)} \quad (9)$$

Theorem 8. $\Phi_{\mathbb{M}}^{(n)}$ is a signed measure over $\mathbb{S} \times \mathbb{M}$.

Its total variation is $|\Phi_{\mathbb{M}}^{(n)}|$ and $\forall n \in \mathbb{N}$, $\Phi_{\mathbb{M}}^{(n)} \ll \mathcal{S} \otimes \mathcal{M}$.

We write $\varphi_{\mathbb{M}}^{(n)} = \frac{d\Phi_{\mathbb{M}}^{(n)}}{d\mathcal{S} \otimes \mathcal{M}}$.

Remark 1. If S is an open set in \mathbb{S} , $\Phi_{\mathbb{M}}^{(n)}(S, \cdot)$ is a signed measure over \mathbb{M} .

Its total variation is $|\Phi_{\mathbb{M}}^{(n)}(S, \cdot)|$ and $\forall n \in \mathbb{N}$, $\Phi_{\mathbb{M}}^{(n)}(S, \cdot) \ll \mathcal{M}$.

We write $\varphi_{\mathbb{M}}^{(n)}(S, \cdot) = \frac{d\Phi_{\mathbb{M}}^{(n)}(S, \cdot)}{d\mathcal{M}}$

Remark 2. $\varphi_{\mathbb{M}}^{(n)}$ is degenerated:

if $x \in \Omega$, $\left\{ s \in \mathbb{S}, x \in r_s^{(n)} \right\}$ is finite. By writing $K(x)$ the size of this set and $s_1(x), \dots, s_{K(x)}(x)$ its elements, there exist $S_1(x), \dots, S_{K(x)}(x)$ open sets of \mathbb{S} such as:

$$\varphi_{\mathbb{M}}^{(n)}(s, x) = \sum_{k=1}^{K(x)} \varphi_{\mathbb{M}}^{(n)}(S_k(x), x) \delta(s - s_k) \quad (10)$$

Theorem 9. If S is an open set in \mathbb{S} and if $V_\epsilon(x)$ is a neighborhood system of x indexed by $\epsilon > 0$, with $\lim_{\epsilon \rightarrow 0} \text{diam}(V_\epsilon(x)) = 0$ then

$$\varphi_{\mathbb{M}}^{(n)}(S, x) = \lim_{\epsilon \rightarrow 0} \frac{\Phi_{\mathbb{M}}^{(n)}(S, V_\epsilon(x))}{\mathcal{M}(V_\epsilon(x))} \quad (11)$$

Theorem 10. If \mathbb{M} is a closed surface and S an open set in \mathbb{S} , $\forall n \in \mathbb{N}$, $\Phi_{\mathbb{M}}^{(n)}(S, \mathbb{M}) = 0$.

Theorem 11. Let S an open set in \mathbb{S} .

There exist $\varphi_S^{(n)} : \Omega \rightarrow \mathbb{R}_+$ and $\vec{d}_S^{(n)} : \Omega \rightarrow \mathbb{U}^2$ the two dimensional unitary sphere in \mathbb{R}^3 , continuous function such as for all $x \in \Omega$ and for all affine plane $\mathbb{M} \ni x$ orthogonal to the direction $\vec{m} \in \mathbb{U}^2$, $\varphi_S^{(n)}$ and $\vec{d}_S^{(n)}$ are integrable over \mathbb{M} and

$$\varphi_{\mathbb{M}}^{(n)}(S, x) = \left\langle \varphi_S^{(n)}(x) \vec{d}_S^{(n)}(x) \middle| \vec{m} \right\rangle \quad (12)$$

If $\varphi_{\mathbb{M}}^{(n)}(S, x) \neq 0$, $\varphi_S^{(n)}(x)$ and $\vec{d}_S^{(n)}(x)$ are unique.

Moreover in that case, there is a positive finite number $K \geq 1$ of elements of S , s_1, \dots, s_K , for all $k \leq K$, $x \in r_{s_k}^{(n)}$, each one being associated to an open set $S_k \ni s_k$ included in S , such as

$$\varphi_S^{(n)} \vec{d}_S^{(n)} = \sum_{k=1}^K \varphi_{S_k}^{(n)}(x) \vec{r}_{s_k}^{(n)}(x) \quad (13)$$

Definition 19. Let $\gamma \in \mathbb{R}$, $|\gamma| < 1$.

For all $x \in \Omega$, we define:

- The total flow: $\Phi_{\mathbb{M}}(M) = \sum_n \gamma^n \Phi_{\mathbb{M}}^{(n)}(\Delta\mathbb{S}, M)$
- The elementary flow: $\varphi_{\mathbb{M}}(x) = \sum_n \gamma^n \int_{\Delta\mathbb{S}} \varphi_{\mathbb{M}}^{(n)}(s, x) \mathcal{S}(ds)$
- The Poyning vector: $\vec{\Pi}(x) = \sum_n \gamma^n \varphi_S^{(n)}(x) \vec{d}_S^{(n)}(x)$
- The power: $P(x) = \left\| \vec{\Pi}(x) \right\|$

Theorem 12. The quantities defined in def. 19 are bonded by the relationships:

- $\Phi_{\mathbb{M}} \ll \mathcal{M}$ and $\frac{d\Phi_{\mathbb{M}}}{d\mathcal{M}} = \varphi_{\mathbb{M}}(x)$
- If $\vec{m}(x)$ is the orthogonal direction to \mathbb{M} at point x , $\varphi_{\mathbb{M}}(x) = \left\langle \vec{\Pi}(x) \middle| \vec{m}(x) \right\rangle$

4.3. Power estimation

Definition 20 (Power estimator). Let $x \in \Omega$ and $M \ni x$ an affine plane orthogonal to some direction \vec{m} and $V_\epsilon(x)$ a neighborhood system of x in \mathbb{M} with $\text{diam}V_\epsilon(x) \rightarrow_{\epsilon \rightarrow 0} 0$.

Let $N \in \mathbb{N}^*$ and $s_1, \dots, s_N \in \Delta\mathbb{S}$, N independent random variables sampled from $\Delta\mathbb{S}$.

$\forall i \leq N$, we write $q^{(n)}(i) = \{\vec{d}_i^{(n)}\}$ if $r_{s_i}^{(n)} \cap V_\epsilon(x) \neq \emptyset$, $q^{(n)}(s_i) = \emptyset$ otherwise.

The power estimator in x , $\hat{P}_{\epsilon, \vec{m}, N}(x)$ is defined by:

$$\hat{P}_{\epsilon, \vec{m}, N}(x) = \frac{1}{N \cdot \mathcal{M}(V_\epsilon(x))} \left\| \sum_{i=1}^N \sum_{n=0}^{\infty} \sum_{\vec{d}_i^{(n)} \in q_i^{(n)}} \gamma^n \frac{\vec{d}_i^{(n)}}{\left\langle \vec{d}_i^{(n)} \middle| \vec{m} \right\rangle} \right\| \quad (14)$$

Theorem 13 (Monte-Carlo ray-tracing). For almost every direction $\vec{m} \in \mathbb{U}^2$, $\hat{P}_{\epsilon, \vec{m}, N}$ converges almost surely to $\hat{P}(x)$ as $N \rightarrow \infty$ and $\epsilon \rightarrow 0$.

Of course, in practice, the limit is not reachable. We will set ϵ small compared to the typical variation distance of the problem and N large enough to ensure the resulting variability of the estimator is consistent with the target application.

This variability is investigated in the next section.

4.4. Variance reduction

To assess the accuracy of the previously defined estimators, we place in the simplest configuration where:

- ∂E is reduced to the ground i.e. the plan of equation $z = 0$ also denoted \mathbb{M} ,
- the antenna \mathbb{S} is place above the origin of \mathbb{M} , at a height $H > 0$,
- it emits uniformly in a portion $\Delta\mathbb{S}$ delimited by $\theta_{xy} \in [0, 2\pi]$, $\theta_z \in]\theta_{z0} - \delta\theta_z, \theta_{z0} + \delta\theta_z[$, with $\theta_{z0} - \delta\theta_z > 0$ and $\theta_{z0} + \delta\theta_z \leq \pi/2$, $\delta\theta_z > 0$.

The uniform measure over $\Delta\mathbb{S}$ is $\Delta\mathcal{S}(d\theta_{xy}, d\theta_z) = \frac{1}{C_{\Delta\mathbb{S}}} d\theta_{xy} |\sin d\theta_z|$ with $C_{\Delta\mathbb{S}} = 4\pi \sin \delta\theta_z \cos \theta_{z0}$.

We evaluate the estimators at a ground level point $x \in \mathbb{M}$.

For all $s \in \Delta\mathbb{S}$, r_s reaches \mathbb{M} one and only one time. Thus the application $r : \Delta\mathbb{S} \rightarrow \mathbb{M}; s \rightarrow r_s \cap \mathbb{M}$ is an injection.

The image of $\Delta\mathbb{S}$ is an open subset of \mathbb{M} denoted $\Delta\mathbb{M}$ corresponding to the crown centered in 0, of internal radius $H/\tan \theta_{z0} + \delta\theta_z$ and external radius $H/\tan \theta_{z0} - \delta\theta_z$.

For numerical applications, we will consider in what follows $H = 20\text{m}$, the estimations at position x are done from a square $V(x)$ with area 100m^2 and $\theta_{z0}, \delta\theta_z$ such as $\Delta\mathbb{M}$ has an internal radius of 50m and an external radius of 1km .

Theorem 14. $r : \Delta\mathbb{S} \rightarrow \Delta\mathbb{M}$ is a C^1 -differomorphism.

It's Jacobian matrix at $s \in \Delta\mathbb{S}$ is denoted $J_r(s)$ and $|\det J_r(s = (\theta_{xy}, \theta_z))| = H^2 \cdot \frac{\cos \theta_z}{\sin^3 \theta_z}$

Let $V(x)$ be a (small) Borelian set surrounding $x \in \Delta\mathbb{M}$. The flow through $V(x)$ is $\Phi(V(x)) = \frac{\Phi(V(x))}{\mathcal{M}(V(x)) \sin \theta_z(x)}$ and the power in x is approximate by $P(V(x)) = \frac{\Phi(V(x))}{\mathcal{M}(V(x)) \sin \theta_z(x)}$

Theorem 15. If $N \in \mathbb{N}^*$, s_1, \dots, s_N are independent random variable drawn on $\Delta\mathbb{S}$ with respect to $\Delta\mathcal{S}$ then

$$\hat{\Phi}(V(x)) = \frac{1}{N} \sum_{i=1}^N \mathbf{1}_{V(x)}(r(s_i)) \quad (15)$$

is an unbiased estimator for $\Phi(V(x))$.

We will use $\hat{P}(x) \simeq \hat{P}(V(x)) = \frac{\hat{\Phi}(V(x))}{\mathcal{M}(V(x)) \sin \theta_z(x)}$ as an estimator of P .

Definition 21. If X is a random variable over some probability space with finite expectancy and variance, the relative variation of X is defined by

$$\sigma_r(X) = \frac{\sqrt{\mathbb{V}X}}{\mathbb{E}X} \quad (16)$$

Theorem 16. The variance of $\hat{\Phi}(V(x))$ is $\mathbb{V}(\hat{\Phi}(V(x))) = \frac{\Phi(1-\Phi)}{N}$; the relative variation of $\hat{\Phi}(V(x))$ and $\hat{P}(V(x))$ are the same and is worth

$$\sigma_r = \sqrt{\frac{1-\Phi}{N\Phi}} \quad (17)$$

In the limit case where $\Phi \ll 1$ and $\mathcal{M}(V(x)) \ll H^2$, $\sigma_r \simeq \frac{1}{\sqrt{N\Phi}}$ and

$$\begin{aligned} \Phi(V(x)) &\simeq \cos r^{-1}(x) |\det J_r(r^{-1}(x))|^{-1} \frac{\mathcal{M}(V(x))}{C_{\Delta\mathbb{S}}} \\ \sigma_r &\simeq \sqrt{\frac{C_{\Delta\mathbb{S}} H^2}{N \sin^3 x \mathcal{M}(V(x))}} \simeq \|x\|^{1.5} \sqrt{\frac{C_{\Delta\mathbb{S}}}{NH \mathcal{M}(V(x))}} \end{aligned}$$

Numerically, we can afford to simulate up to $N = 10^7$ rays this result implies that next to the internal radius of the crown, $\sigma_r \gtrsim 0.4\%$ and next to the external radius, $\sigma_r \gtrsim 33\%$.

In what follows, we design an importance sampling to homogenize the relative variation through space.

Theorem 17. If \mathcal{T} is a measure over $\Delta\mathbb{S}$ such as $\mathcal{T}(\Delta\mathbb{S}) = 1$ and $\mathcal{S} \ll \mathcal{T}$, we write $\omega(s) = \frac{d\mathcal{S}}{d\mathcal{T}}$.

Let $N \in \mathbb{N}^*$, s_1, \dots, s_N random points of $\Delta\mathbb{S}$ drawn with respect to \mathcal{T} then an estimator of $\Phi(V(x))$ is given by:

$$\hat{\Phi}_{\mathcal{T}} = \frac{1}{N} \sum_{i=1}^N \mathbf{1}_{V(x)}(r(s_i)) \omega(s_i) \quad (18)$$

Furthermore, $\mathbb{E}\hat{\Phi}_{\mathcal{T}}^2 = \int_{\Delta\mathbb{S}} \mathbf{1}_{V(x)}(r(s)) \omega^2(s) \mathcal{T}(ds)$. If $\mathcal{T} \ll ds = d\theta_{xy} d\theta_z$,

$$\mathbb{E}\hat{\Phi}_{\mathcal{T}}^2 = \int_{\Delta\mathbb{M}} \mathbf{1}_{V(x)}(y) \omega^2(r^{-1}(y)) |\det J_r(r^{-1}(y))|^{-1} \frac{d\mathcal{T}}{ds}(r^{-1}(y)) \mathcal{M}(dy) \quad (19)$$

From th. 17 we can provide an approximation of $\mathbb{E}\hat{\Phi}_{\mathcal{T}}^2$ and $\sigma_r(\hat{\Phi}_{\mathcal{T}}$ in the limit case where $\Phi \ll 1$ and $\mathcal{M}(V(x)) \ll H^2$ (and $\mathcal{T} \ll ds$):

$$\mathbb{E}\hat{\Phi}_{\mathcal{T}}^2 \simeq \omega^2(r^{-1}(x)) |\det J_r(r^{-1}(x))|^{-1} \frac{d\mathcal{T}}{ds}(r^{-1}(x)) \mathcal{M}(V(x)) \quad (20)$$

$$\sigma_r(\hat{\Phi}_{\mathcal{T}}) \simeq \tilde{\sigma}_r(x) \stackrel{\text{def}}{=} \sqrt{\frac{|\det J_r(r^{-1}(x))|}{\frac{d\mathcal{T}}{ds}(r^{-1}(x)) \mathcal{M}(V(x))}} \quad (21)$$

We want to design a measure \mathcal{T} such as

- the sampling according to \mathcal{T} is feasible without computation overload (for instance by using the inverse method),
- the relative variations are sensibly equal through space and the lowest possible

The choice of \mathcal{T} maximizing $\int \tilde{\sigma}_r^{-1}(x) dx$ leads to a \mathcal{T} known under closed form:

Theorem 18. The maximum of $\int_{\Delta\mathbb{M}} \tilde{\sigma}_r^{-1}(x) dx$ over measures \mathcal{T} , $\mathcal{T}(\Delta\mathbb{M}) = 1$, $\mathcal{S} \ll \mathcal{T} \ll d\theta_{xy} d\theta_z$ is reached for $d\mathcal{T} = \frac{1}{C_{\mathcal{T}}} d\theta_{xy} \frac{1}{H^2} |\det J_r(\theta_z)| d\theta_z = \frac{1}{C_{\mathcal{T}}} d\theta_{xy} F(d\theta_z)$ with

$$F(\theta_z) = \frac{1}{\sin^2 \theta_{z_0} - \delta\theta_z} - \frac{1}{\sin^2 \theta_z} \quad (22)$$

$$C_{\mathcal{T}} = \pi \left(\frac{1}{\sin^2 \theta_{z_0} - \delta\theta_z} - \frac{1}{\sin^2 \theta_{z_0} + \delta\theta_z} \right) = \frac{\mathcal{M}(\Delta\mathbb{M})}{H^2} \quad (23)$$

Thus basically, the relative variation under \mathcal{M} is independent of the position and is worth

$$\sigma_r \simeq \sqrt{\frac{\mathcal{M}(V(x))}{N \mathcal{M}(\Delta\mathbb{M})}} \quad (24)$$

This implies that for $N = 10^7$ rays sampled from \mathcal{T} , $\sigma_r \simeq 5\%$ at every point of $\Delta\mathbb{M}$.

5. Results

The mapping of each point in an horizontal plane the power at this point is called an attenuation map. In practice, the attenuation map is estimated from pixels surrounding a discrete set of points called evaluation points.

For instance, Fig.4, plots the estimated attenuation map for a simulated Crack-STIT city in a disc of radius 1.5km. The antenna is placed above the roof whose barycenter is the closest to the origin. The evaluation points $x_{j,k}$ have been chosen to form crowns of regularly spaced radius and sectors of constant aperture: $x_{j,k}$ is at the distance $j\delta d$ of the center and forms an angle $k\delta\alpha$ with the x -axis. The pixels are arc of crowns surrounding the evaluation point to form a partition of the space.

We notice on this map that:

- the power is globally decreasing with the distance
- some area are shadowed by the buildings
- long streets passing next to the antenna behave as wave guides.

To assess the expectancy of power in the street zone, we generate N maps with the same morphological parameters. For each map i we compute the attenuation map $(P_i(d_j, \alpha_k))_{j,k}$. A pixel that is not at least partially in the street has a power 0.

$$\hat{P}(d_j) = \sum_k \sum_i P_i(d_j, \alpha_k) \eta_i \frac{\delta\alpha}{N \cdot 2\pi} \quad (25)$$

where η_i the the street area fraction in the simulation window of map i and $\delta\alpha$ is the angular opening of pixels.

Notice that by sum permutation in the above formula, for a particular map, all the pixels in the crown at the distance d_j are averaged, since there are typically 200 pixels in this crown, the relative error in the estimation of $P_i(d_j)$ is 14 times smaller than the relative error in the estimation of the power in a particular pixel.

We have generated for six cases (PLT and Crack STIT both with anisotropy coefficient of 0.5 and 1) 1000 cities in a disc of radius $R + \Delta R = 1.5\text{km}$ and estimated the power density in the disc of radius R to avoid side-effects.

We obtain estimations of the expected power observed at a certain distance of the source for the different cities' morphology.

The estimated functions $P(d)$ are fitted by the model $P(d) = A/d^\alpha$ (fig.5). The smallest fits' R^2 -index is 0.99909. The order of weight of α is significantly smaller for PLT (around 3.7) than for Crack (around 4.6) whereas the anisotropy coefficient has only a slight influence. At least at a distance equal to twice the typical radius of a serving zone in a cellular network, the path-loss is thus a power function as pointed out empirically in [17].

6. Conclusion

In this paper we have presented a unified stochastic geometry and ray-tracing framework. This framework has been efficiently implemented in C++ under the name *GeoStat*.

The models of city we have proposed, can be calibrated to fit real world map from simple mean formulas. It mimic main features of real cities like 3D geometry whose propagation properties differs essentially from 2D's ones, façade alignments along streets that produce wave guide phenomena or organization of buildings into blocks producing wave concentration.

We have presented a mathematical framework to define and compute properly classical physical quantities in a probabilistic fashion. This framework is general and can be easily adapte to take into account waves interference or propagation schemes different from those of optical geometry.

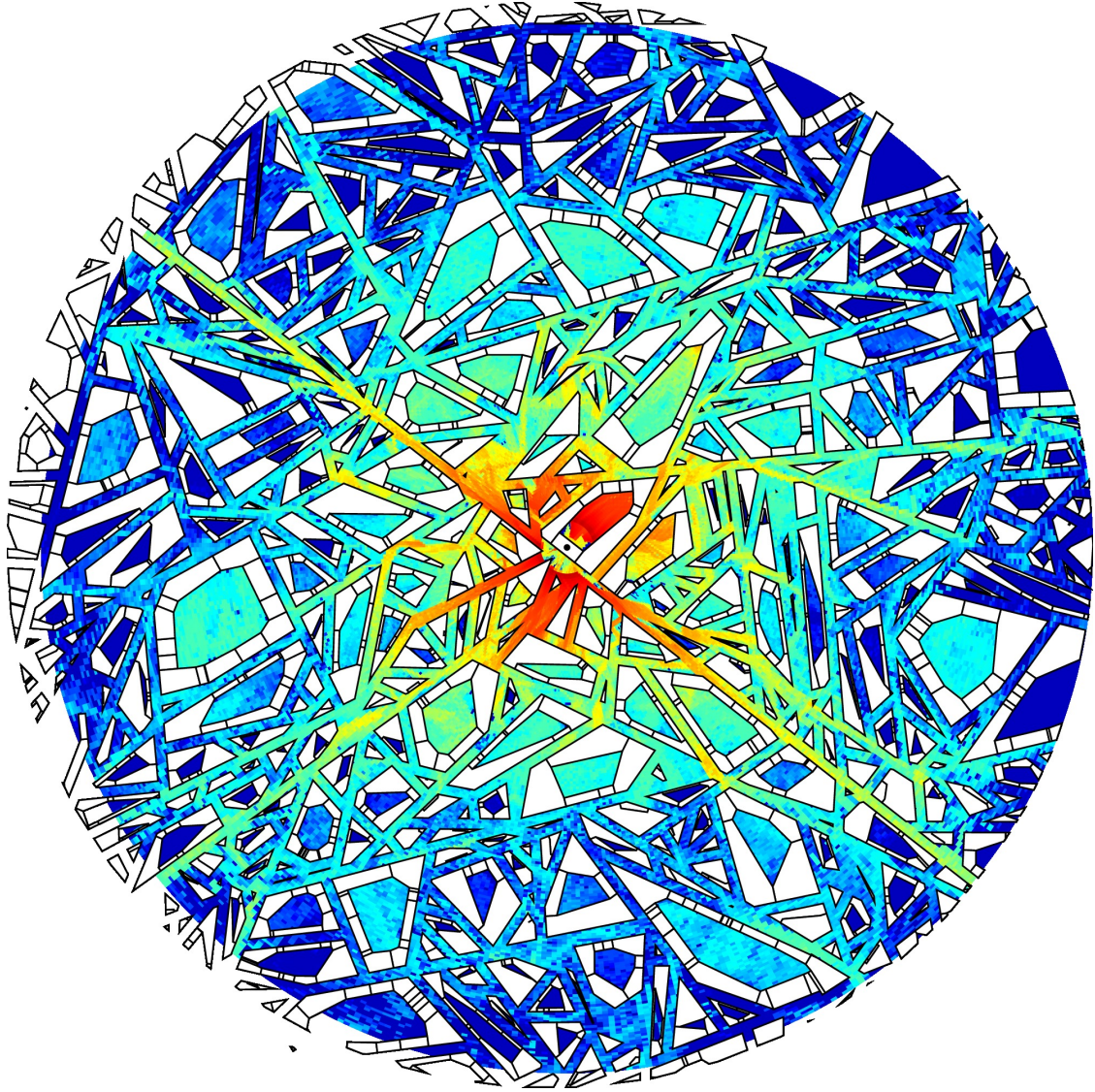


Figure 4: Estimation of the attenuation map of a random Crack Stit city with typical realistic tunings of Appendix A. (Colors represent the logarithm of the power density).

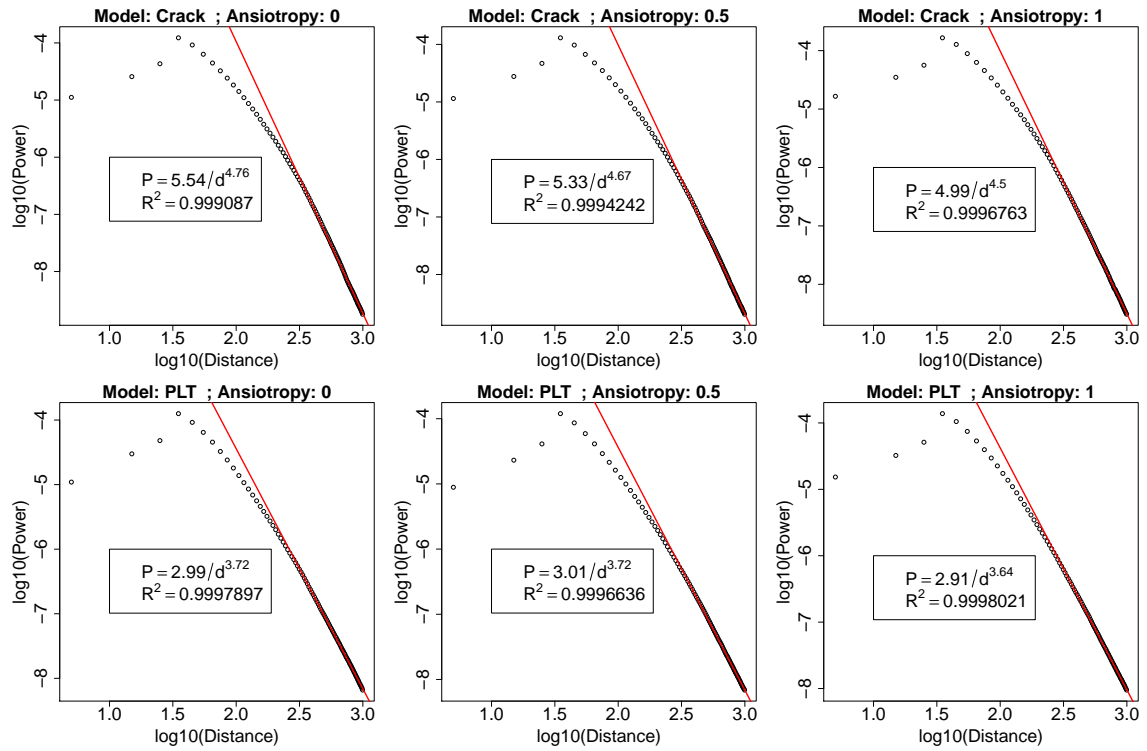


Figure 5: log-log plots of the mean power received at a distance d for Crack (first row) and PLT (second row). The anisotropy coefficient is 0, 0.5 and 1 from left to right. The fitting by a power function is satisfactory. The attenuation exponent is different for the two classes of tessellations: around 4.6 for Crack and around 3.7 for PLT, the latest being a better environment for wave to propagate. The anisotropy does not have a strong influence on the attenuation of the wave.

As an instance of application, we have validated in this paper that the path-loss function is a power function whose attenuation exponent is related to the morphology of the environment at least in the range of distances relevant for telecommunication engineering. A more precise discussion has been presented in [22]. Other applications such as Sub-Channel distribution has also already been investigated in [23] using *GeoStat* framework.

Appendix A. Parameter summary

Here is the summary of the model's parameters and of their notation. To each one is associated a typical numerical value which is used at the different stages of the simulation. We distinguish physical parameters (-) from technical ones (+).

- Simulation window
 - + $R = 1$ km: radius of the circular window W .
 - + $\Delta R = 500$ m: offset radius to avoid side effects.
- Tessellation
 - $U_2 = 400$ m: mean perimeter of the typical block of houses.
- Buildings
 - $l = 10$ m: street thickness.
 - $h = 15$ m: mean height of a building.
 - $b = 10$ m: mean length of a building facade.
- Antenna
 - $P_0 = 40$ W: total power of the source.
 - $f = 2 \cdot 10^9$ Hz, $\lambda = 15$ cm: frequency and wave length (GSM).
 - $\theta_0 = \pi/2$ rad, $\Delta\theta = \pi$ rad: horizontal aperture of the source.
 - $\varphi_0 = \pi/12$ rad, $\Delta\varphi = \pi/12$ rad: vertical aperture of the source
- Rays
 - + $N = 10^7$: number of rays used in a simulation.
 - $n = \infty$: maximum number of reflections for a ray.
 - $1/\gamma = 0.5 = -3$ dB: power gain after a reflection.
- Statistics
 - + $R = 1$ km: radius of the measurement grid.
 - + $\delta d = 10$ m: radial length of a pixel.
 - + $\delta\alpha = 2$ degrees: angular opening of a pixel.

Appendix B. Construction of random tessellations

We present in this annex the gist of the implementation of the algorithms simulating random tessellations.

Appendix B.1. Data structures and division functions

Appendix B.1.1. Polygons - Simple Data structures

We implement a line, half-line and segment structures that drift from an abstract **edge** class.

From an edge e , we can create the opposite edge $-e$ with the same support and the opposite orientation.

A **circular list** cl is a collection of homogeneous objects $cl = (O_1, \dots, O_n)$ with an iterator it that can be initialized to any O_i , $1 \leq i \leq n$, if at a moment, it 's state is O_j then $it.next() = O_{j+1}$ if $j < n$ or $it.next() = O_1$ if $j = n$.

A **convex polygon** is represented by its border, that is to say a circular list of edges (e_1, \dots, e_n) . The integrity of a polygon is ensured by considering edges e_i with the same orientation and sorting them clockwise.

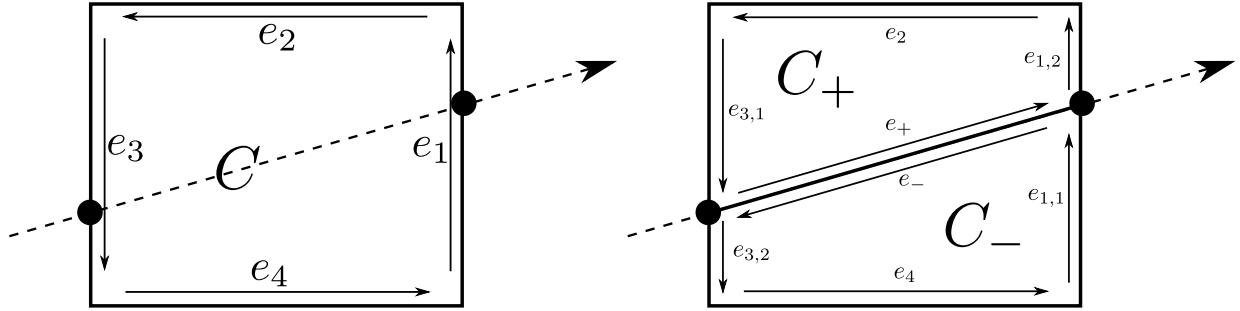


Figure B.6: Division of polygon C by a line into two polygons C_+ and C_- . In a first step, we look for intersection points p_1 and p_2 . Borders of C are rewritten by introducing these points and then C_+ and C_- can be described by the sequence of their edges.

Appendix B.1.2. Division of a polygon by a line

The algorithm of division of a polygon C by a line L simply consists in finding intersections between L with the edges of C . If there are no intersection, **divide** returns (C, \emptyset) or (\emptyset, C) according to the position of C relatively to L . (**Intersection finding step**).

The most common case is when L intersects two edges (Fig.B.6). In this case we write (f_1, p_1) and (f_2, p_2) the intersected edges associated to their intersection points with L . Indexes are chosen in such a way that $\overrightarrow{p_1 p_2}$ has the same orientation as L . Edges $f_i, i = 1, 2$ give birth to two new edges f_{i1} and f_{i2} with the same orientation as f_i . Polygon C that wrote $(e_1, \dots, e_k = f_1, \dots, e_l = f_2, \dots, e_n)$ (it is always possible to brought back to this representation of the polygon by circular shift of the edges) can be rewritten $(e_1, \dots, f_{1,1}, f_{1,2}, \dots, f_{2,1}, f_{2,2}, \dots, e_n)$. (**Rewriting step**).

One creates two new segments: $e_+ = [p_1, p_2]$ and $e_- = -e_+$. Polygons C_+ and C_- resulting from the division can be formally written as : $C_+ = (e_+, f_{1,2}, \dots, f_{2,1})$ and $C_- = (e_-, f_{2,2}, \dots, f_{1,1})$. (**Bridge step**).

The case when a single edge is intersected corresponds to the division of an infinite polygon into two infinite polygons and can be easily written in the same spirit as the previous case.

Appendix B.1.3. Tessellation - Complex Data structures

If the tessellation is seen as a collection of polygons, two problems raise when one wants to divide this tessellation by a line.

- It would be necessary to treat the division of each polygon although solely a fraction of the polygons will be actually divided (if the order of magnitude of the number of polygons is n , the order of magnitude of divided polygons is \sqrt{n}).
- The independent divisions of two polygons that share an edge that is cut into a point p produces two new points p_1 and p_2 theoretically equal but that would not have the same reference in the program execution and that for numerical problems could have a positive distance.

To solve these problems, we make a slight change in data structure: edges are replaced by **edgeContainers** (a structure containing an edge, a pointer to the cell it belongs to and a pointer to the edgeContainer containing its opposite edge) and polygons by **cells** (a circular list of edgeContainers), a tessellation is then a list of cells:

- **edgeContainer**
 - Edge * edge
 - edgeContainer * opposite
 - Cell * left
- **Cell**

– Circular list of edgeContainer

• **Tessellation**

– List of cells

When a cell is divided (Algo.1),it is possible to list adjacent cells that are also divided, to update them and to divide them knowing the structures that have been added in the previous cell division (Algo.2).

Algorithm 1 $\mathbf{division}(C, L, \Xi)$. C : cell, L : line, Ξ : tessellation

Intersection step

1: Find edgeContainer $ec_1, ec_2 \in C \mid L \cap ec_1.\mathbf{edge} = p_1: L \cap ec_2.\mathbf{edge} = p_2$

Update

2: $\forall i = 1, 2$ cut ec_i by p_i into ec_{i1} and ec_{i2}
3: Rewrite C in consequence.
4: $\forall i, j$ $ec_{ij}.\mathbf{opposite} \leftarrow ec_i.\mathbf{opposite}$
5: Create $\forall i, j$ $\text{minusec}_{ij} = -ec_{ij}$
6: Replace $ec_i.\mathbf{opposite}$ by $\text{minusec}_{i2}, \text{minusec}_{i1}$ in $ec_i.\mathbf{opposite}.\mathbf{left}$
7: $\forall i, j$ $\text{minusec}_{ij}.\mathbf{opposite} = ec_{ij}$

Bridge step

8: Exchange p_1 and $p_2 \mid \langle \overrightarrow{p_1 p_2} \mid L \rangle > 0$ if necessary
9: Create edgeContainer ec_+ and ec_- ; $ec_+.\mathbf{opposite} = ec_-$ and conversely.
10: Create C_+ and C_-
11: $\forall ec \in C_+, ec.\mathbf{left} = C_+$ idem in C_-

Tessellation updating

12: $\Xi = (\Xi \setminus C) \cup \{C_+, C_-\}$

Recursive call of the function division

13: $\mathbf{division}(ec_1.\mathbf{opposite}.\mathbf{left}, L, \Xi, p_1, \text{minusec}_{1,2})$ (Algo.2)
14: $\mathbf{division}(ec_2.\mathbf{opposite}.\mathbf{left}, L, \Xi, p_2, \text{minusec}_{2,2})$ (Algo.2)

If there is no intersection, the recursion stops. The division of a tessellation Ξ by a line L goes back to find a cell C_0 divided by L and to call $\mathbf{division}(C_0, L, \Xi)$.

Appendix B.2. Random line simulation

The tessellations under consideration are constructed from iterated divisions of a polygon by random lines. The following properties allow simulating a random line hitting a given polygon with a probability 1:

Theorem 19. If C is a circle with radius r then $\#\mathcal{L}_C(\cdot)$ follows a Poisson Law of parameter $\lambda.2.r$ whatever \mathcal{R} is and conditionally to it cuts C , a line of the process has a distance to the center of C uniformly distributed.

Theorem 20. If $W \subset C$ then $\mathcal{L}_W(\cdot) = \mathcal{L}_{W \cap C}(\cdot) = \mathcal{L}_C(\cdot \cap W)$.

Consequently, it is sufficient to draw a Poisson Line in C and keep only lines that cross W (Algo.3). The choice of the smallest circle circumscribed to W permits to minimize line rejections and thus to improve running time.

Algorithm 2 $\text{division}(C, L, \Xi, p_0, ec_0)$ C : cell, L : line, Ξ : tessellation, p_0 : point in ec_0 an edgeContainer.

Intersection points

- 1: $p_1 = p_0, ec_1 = ec_0$
- 2: Find $ec' = ec_2 \mid L \cap ec_2.\text{edge} = p', p_2, ec_2 \neq ec_1, \neq ec_1.\text{next}$
- 3: Cut ec_2 by p_2 into ec_{21} and ec_{22}

Updating step

- 4: $\forall i$ cut ec_i by p_i into ec_{i1} and ec_{i2}
- 5: Rewrite C in consequence.
- 6: $\forall i, j$ $ec_{ij}.\text{opposite} \leftarrow ec_i.\text{opposite}$
- 7: Create $\forall i, j$ $\text{minusec}_{ij} = -ec_{ij}$
- 8: Replace $ec_i.\text{opposite}$ by $\text{minusec}_{i2}, \text{minusec}_{i1}$ in $ec_i.\text{opposite.left}$
- 9: $\forall i, j$ $\text{minusec}_{ij}.\text{opposite} = ec_{ij}$

Bridge step

- 10: Exchange p_1 and $p_2 \mid \langle p_1 p_2 \mid L \rangle > 0$ if necessary
- 11: Create edgeContainer ec_+ and ec_- ; $ec_+.\text{opposite} = ec_-$ and conversely.
- 12: Create C_+ and C_-
- 13: $\forall ec \in C_+, ec.\text{left} = C_+$ idem in C_-

Tessellation updating

- 14: $\Xi = \Xi \setminus C \cup \{C_+, C_-\}$

Recursive call of the function division

- 15: $\text{division}(ec'.\text{opposite.left}, L, \Xi, p', \text{minusec}_{2,2})$
-

Algorithm 3 $l \sim \mathcal{L}_W$ Random line in W

- 1: INPUT W
 - 2: Inscribe W in a circle of center $0'$ and radius $r..$
 - 3: **while do**
 - 4: $r_0 \sim \mathcal{U}_{[-r,r]}$; $\alpha \sim \mathcal{R}$
 - 5: Consider the line $l = (r_0, \alpha) + 0'$
 - 6: **if** $d \cap W \neq \emptyset$ **then return** l
 - 7: BREAK
 - 8: **end if**
 - 9: **end while**
-

Appendix B.3. Algorithms for random line generated processes

The division functions (Algo.1, 2) and the random line simulation (Algo.3) based on th. 19, th. 20 lead to the simple algorithm 4 to simulate the intersection of a PLT with a compact connected window W .

The Crack's construction can be made recursively with the function **division** and a generator of the law \mathcal{L}_ω with ω a compact set.

To this we define the auxiliary function of evolution of a cell C belonging to a tessellation Ξ from a time $t > 0$:

The theorem def. 13 rewrites then computationally as:

Definition 22. There exist a stationary, locally finite tessellation whose intersection with a convex and compact window W is the result of $\text{crack}(W, \tau, \lambda) = \text{evolution}(W, 0 \mid \{W\}, \tau, \lambda)$. It is called the Crack STIT tessellation.

Algorithm 4 $\Xi = \text{PLT}(\lambda, W)$ Poisson Line Tessellation process intersected by W

```
1: INPUT  $\lambda \in \mathbb{R}_+, W$ 
2: OUTPUT: Tessellation  $\mathbf{T}$ 
3: Tessellation  $\mathbf{T}_0 = \{W\}$ 
4: Inscribe  $W$  in a circle of center  $O'$  and radius  $r$ .
5:  $N \sim \mathcal{P}(\lambda \cdot 2r)$ ;  $n = 1$ 
6: while  $n \leq N$  do
7:    $r_0 \sim \mathcal{U}_{[-r, r]}$ ;  $\alpha \sim \mathcal{R}$ 
8:   Consider the line  $l = (r_0, \alpha) + O'$ 
9:   if  $d \cap W \neq \emptyset$  then
10:     $\Xi_n = \text{division}(\Xi, l)$ 
11:     $n++$ 
12:   else
13:     $\Xi_n = \mathbf{T}_{n-1}$ 
14:   end if
15: end while
16:  $\Xi = \Xi_N$ 
```

Algorithm 5 $\text{evolution}(C, t, \Xi, \tau, \lambda)$

```
1:  $\delta t \sim \mathcal{E}(\lambda \cdot \nu(C))$ 
2: if  $t + \delta t < \tau$  then
3:    $L \sim \mathcal{R}_C, (C_+, C_-) = \text{division}(C, L)$ 
4:    $\Xi = (\Xi - \{C\}) \cup \{C_+, C_-\}$ 
5:   evolution $(C_+, t + \delta t, \Xi, \tau, \lambda)$ 
6:   evolution $(C_-, t + \delta t, \Xi, \tau, \lambda)$ 
7: end if
```

Appendix B.4. Running resources

To optimize the ray-tracing algorithm, we use a structure that divides recursively the plane into 4^M squared regions. Each region contains a list of references to the buildings that intersect them. If M is well chosen, this technique permits to reduce the ray tracing complexity: it becomes almost independent of the number of buildings. It calls for a preprocessing step that can be performed in $\Theta(\log M \cdot N)$. The table B.2 sums up the complexity of algorithms at the different steps of the simulation and their average running time on a 32 and 64 bit computer. The most greedy step is the propagation simulation by ray-tracing. The simulation time order of weight is $1.8 \cdot 10^{-3} N$ s with N the number of rays, other steps being negligible from $4 \cdot 10^5$ rays. Nonetheless in some particular cases (the antenna is very high or all the buildings have the same height) the algorithm can be improved and the time order of weight decreases to $2 \cdot 10^{-4} N$ s.

From a memory point of view, the simulation does not require a lot of resources since rays can be destroyed once their trajectory computation is over and measurement pixels have been updated.

References

- [1] François Baccelli and Bartłomiej Błaszczyszyn. *Stochastic Geometry and Wireless Networks, Part I: Theory*. Now Publishers Inc, 2009.
- [2] François Baccelli and Bartłomiej Błaszczyszyn. *Stochastic Geometry and Wireless Networks, Part II: Applications*. Now Publishers Inc, 2009.
- [3] François Baccelli, Maurice Klein, Marc Lebourges, and Serguei Zuyev. Stochastic geometry and architecture of communication networks. *J. Telecommunication Systems*, 7:209–227, 1995.
- [4] M.F. Catedra, J. Perez, F. Saez de Adana, and O. Gutierrez. Efficient ray-tracing techniques for three-dimensional analyses of propagation in mobile communications: application to picocell and microcell scenarios. *Antennas and Propagation Magazine, IEEE*, 40(2):15–28, apr 1998.

Algorithm	Complexity	32 bits	64 bits
Tessellation			
PLT	$(\lambda.r)^{3/2}$	0.1s	0.03 s
Crack	$(\lambda.r)^2$	0.08s	0.02s
Buildings	$\frac{(\lambda.r)^2}{b}$	1.2s	0.25s
Preprocessing	$N \cdot \log M$	5.1s	1.2s
Propagation	N	90 min	22 min
Statistics	N	1.2s	0.4s

Table B.2: Complexity of the different steps of the simulation according to the parameters in Appendix A and the computation time on a computer Linux 32 bits 1.82 GHz, 1Go Ram and a computer Linux 64 bits, 2.93 GHz, 64 Go Ram for typical values of these parameters. The implement has been performed in C++ and compiled by g++ with -O2 option.

- [5] Thomas Courtat, Catherine Gloaguen, and Stephane Douady. Mathematics and morphogenesis of cities: A geometrical approach. *Phys. Rev. E*, 83:036106, Mar 2011.
- [6] Richard Cowan. New classes of random tessellations arising from iterative division of cells. *Adv. in Appl. Probab.*, 42(1):26–47, 2010.
- [7] C. Gloaguen, P. Coupe, R. Maier, and V. Schmidt. Stochastic modelling of urban access networks. In *Proc. 10th Internat. Telecommun. Network Strategy Planning Symp. (Munich, June 2002)*, 2002.
- [8] C. Gloaguen, F. Fleischer, H. Schmidt, and V. Schmidt. Simulation of typical cox-voronoi cells, with a special regard to implementation tests. *Mathematical Methods of Operations Research*, 62:357–373, 2005.
- [9] C. Gloaguen, F. Fleischer, H. Schmidt, and V. Schmidt. Fitting of stochastic telecommunication network models via distance measures and monte-carlo tests. *Telecommun. Syst.*, 31:4, 2006.
- [10] Catherine Gloaguen, Florian Voss, and Volker Schmidt. Parametric distance distributions for fixed access network analysis and planning. In *ITC21*, 2009.
- [11] Wilfrid S. Kendall and Ilya Molchanov, editors. *New perspectives in stochastic geometry*. Oxford Scholarship Online. Oxford University Press, Oxford ; New York, 2010.
- [12] S. Marano and M. Franceschetti. Ray propagation in a random lattice: a maximum entropy, anomalous diffusion process. *Antennas and Propagation, IEEE Transactions on*, 53(6):1888 – 1896, june 2005.
- [13] Frédéric Morlot. A population model based on a poisson line tessellation. In *WiOpt*, pages 337–342, 2012.
- [14] W. Nagel and V. Weiss. Crack stit tessellations : Characterization of stationary random tessellations stable with respect to iteration. *Advances in applied probability*, 37:859–883, 2005.
- [15] W. Nagel and V. Weiss. Mean values for homogeneous stit tessellations in 3d. *Image Anal Stereol*, 27:29–37, 2008.
- [16] Andrea Perna, Pascale Kuntz, and Stéphane Douady. Characterization of spatial networklike patterns from junction geometry. *Phys. Rev. E*, 83:066106, Jun 2011.
- [17] T.K Sarkar, Michael C. Wicks, Salazar-Palma Magdalena, and Robert J Bonneau, editors. *Smart Antennas*. .Wiley Series in Microwave and Optical Engineering, 2010.
- [18] D. Stoyan, W.S. Kendall, and J. Mecke. *Stochastic Geometry and its applications*. J. Wiley & Sons, 1995.
- [19] Q. Sun, S.Y. Tan, and K.C. Teh. Analytical formulae for path loss prediction in urban street grid microcellular environments. *Vehicular Technology, IEEE Transactions on*, 54(4):1251 – 1258, july 2005.
- [20] M. N. M. van Lieshout. *Markov point processes and their applications*. Imperial College Press, 2000.
- [21] Florian Voss, Catherine Gloaguen, and Volker Schmidt. Scaling limits for shortest path lengths along the edges of stationary tessellations. *Adv. in Appl. Probab.*, 42(4):936–952, 2010.
- [22] Xiaoxing Yu, Thomas Courtat, Philippe Martins, Laurent Decreusefond, and Jean-Marc Kelif. Crack stit tessellations for city modeling and impact of terrain topology on wireless propagation. In *WinMeE 2014*, 2014.
- [23] Xiaoxing Yu, Thomas Courtat, Philippe Martins, Laurent Decreusefond, and Jean-Marc Kelif. Research of mobile deployment and sub-channel distribution under terrain topology impact. In *PIMRC*, 2014.